Applied Thermal Engineering 93 (2016) 697–706

Contents lists available at ScienceDirect

Applied Thermal Engineering

journal homepage: www.elsevier.com/locate/apthermeng

Research Paper

CFD investigation on particle deposition in aligned and staggered ribbed duct air flows

Hao Lu, Lin Lu *

Department of Building Services Engineering, The Hong Kong Polytechnic University, Hung Hom, Kowloon, Hong Kong, China

HIGHLIGHTS

- The effects of rib arrangements on particle deposition enhancement are investigated.
- The surface ribs with aligned arrangement have better performance than staggered ones.
- The mechanisms of particle deposition enhancement are analyzed and discussed.
- Pressure drop-weighted deposition enhancement is evaluated for different rib arrangements.

ARTICLE INFO

Article history:
Received 10 August 2015
Accepted 8 October 2015
Available online 19 October 2015

Keywords:
Particle deposition enhancement
Surface rib arrangement
CFD method

ABSTRACT

This study investigated the effects of surface rib arrangements on particle deposition in two-dimensional ribbed duct air flows by CFD method. The turbulent duct air flows were simulated by Reynolds stress model (RSM) with UDF correction, and the particle motions were solved by discrete particle model (DPM). The surface ribs were arranged in aligned or staggered layouts. The air velocity profiles for both smooth and ribbed duct flows as well as the particle deposition velocity for smooth duct cases were all in good agreement with the relative literature data. The simulation results showed that the surface ribs with aligned arrangement have better performance on small particle deposition enhancement, compared with staggered surface ribs. Nevertheless, the large particle deposition rates are not enhanced obviously by both kinds of surface ribs. Considering the flow drag increase, the maximum particle deposition enhancement can reach 425 times for particles with 1 μm diameter. Finally, the mechanisms of particle deposition enhancement by aligned and staggered surface ribs were analyzed and discussed from the views of rib interception, deposition area increase, turbulent eddy capture and the flow passage width. Surface ribs with aligned arrangement are recommended to be applied in particle removal and air clean devices.

1. Introduction

Understanding of particle deposition on the wall from turbulent air flow is crucial for wide industrial processes, such as various particulate removal or air clean equipment [1–3]. In these devices, particle deposition enhancement is necessary and significant to improve the aerosol removal efficiency and performance. It was found that repeated surface ribs, which have been widely applied to enhance heat transfer, are also effective and efficient in particle deposition enhancement [4–6]. The aerosol clean efficiency can be dramatically improved due to the interception of the surface ribs in air electrostatic precipitators (ESP) [7]. In the previous studies conducted by the authors [8,9], it was also found that surface ribs can obviously enhance particle deposition velocity for several orders of magnitude, especially for small particles ($\tau_p^+ < 1$). However, the pressure drop is increased by the surface ribs due to form drag at the same time. Therefore, it is valuable and crucial to find out the optimal rib parameters and arrangements for higher particle deposition enhancement with lower flow drag increase.

Particle deposition in smooth duct air flow had been successfully predicted by Zhao and Chen using Eulerian–Eulerian approach [10] and by Tian and Ahmadi using Eulerian–Lagrangian approach [11]. Othmane et al. [12] and Chorel et al. [13] further investigated the particle deposition mechanisms in duct flow by considering the effects of temperature gradients, surface roughness and computational mesh resolution. Nevertheless, there are few studies carried out on particle deposition enhancement by ribbed surface. Lai et al. [14–16] compared particle deposition rate in smooth and ribbed duct air flows by experimental measurement. The surface ribs are in aligned arrangement. The results indicated that surface rib is a good alternative for particle deposition enhancement. Iacono et al. [17] numerically investigated the effects of particle shapes on deposition characteristics in ribbed channel flows. The surface ribs are also in aligned arrangement. It was found that there is

* Corresponding author. Tel.: +852 34003596; fax: +852 2765 7198.
E-mail address: vivien.lu@polyu.edu.hk (L. Lu).

http://dx.doi.org/10.1016/j.applthermaleng.2015.10.030
1359-4311/

significant difference on the deposition behaviors between spherical and non-spherical particles. Suh and Kim [18] studied the influence of obstructions on particle collection efficiency in EPS. The results showed that the obstructions obviously increase the collection efficiency for small particles. Recently, Barth et al. [19] and Lecrivain et al. [20] investigated multilayer particle deposition in ribbed channel flow with aligned arrangement by experimental measurements and numerical simulation, respectively. Nevertheless, the particle deposition enhancement was not studied. In the previous studies conducted by the authors [8,9], the effects of rib heights and spacing on particle deposition velocity as well as the mechanisms of deposition enhancement were investigated. It was found that surface ribs with smaller heights and spacing have better performance on particle deposition enhancement with lower flow drag increase. However, the effects of rib arrangements on particle deposition enhancement performance have not been investigated and optimized. Different rib arrangements may have significant influences on particle deposition performance. The common arrangements for heat transfer enhancement are aligned or staggered layouts. Therefore, this study aims to investigate particle deposition in ribbed duct air flows with two different rib arrangements: aligned and staggered layouts.

The CFD simulation methods have been a powerful tool to investigate particle deposition in turbulent air flow [21–23]. Compared with experimental measurements, CFD simulation can provide detailed air flow fields and particle behaviors more conveniently [24,25]. However, reasonable numerical models are crucial for correctly simulating the particle deposition process. Reynolds stress model (RSM) with velocity fluctuation correction has been proven to be a more accurate turbulent model for particle deposition prediction than other RANS models [11,26]. This is because RSM model considers turbulent anisotropy while other turbulent models such as k–ε or k–ω models are based on turbulent isotropic hypothesis. For particle motion model, discrete particle model (DPM) is employed to track each particle trajectory. The objective of this study is to investigate and evaluate the effects of rib arrangements on particle deposition enhancement performance. The particle deposition velocity, the flow drag increase and the mechanisms of particle deposition for different particle sizes in aligned and staggered ribbed duct air flows are studied and discussed.

2. Numerical model and methodology

In present study, CFD software ANSYS FLUENT 13.0 with user-defined function (UDF) code corrections was employed to predict particle deposition behaviors in ribbed duct air flows.

2.1. Turbulent air flow and particle motion models

The RSM model was employed to solve turbulent duct air flows. The governing equations for mass and momentum conservation are demonstrated by,

$$\frac{\partial \bar{u}_i}{\partial x_i}=0, \tag{1}$$

$$\frac{\partial \bar{u}_i}{\partial t}+\bar{u}_j\frac{\partial \bar{u}_i}{\partial x_j}=-\frac{1}{\rho}\frac{\partial \bar{p}}{\partial x_i}+\frac{1}{\rho}\frac{\partial}{\partial x_j}\left(\mu\frac{\partial \bar{u}_i}{\partial x_j}-\rho\overline{u_i'u_j'}\right), \tag{2}$$

where $\bar{u}_i$ is the time-averaged velocity. $\bar{p}$ is the time-averaged pressure. $\rho\overline{u_i'u_j'}$ is the Reynolds stress tensor. μ is the dynamic viscosity of the air. The Reynolds stress transport equation can be described by,

$$\frac{\partial}{\partial t}\left(\overline{u_i'u_j'}\right)+\bar{u}_k\frac{\partial}{\partial x_k}\left(\overline{u_i'u_j'}\right)=\underbrace{\frac{\partial}{\partial x_k}\left(\frac{\nu_t}{\sigma_k}\frac{\partial \overline{u_i'u_j'}}{\partial x_k}\right)}_{D_{T,ij}=\text{Turbulent Diffusion}}\underbrace{-\left(\overline{u_i'u_k'}\frac{\partial \bar{u}_j}{\partial x_k}+\overline{u_j'u_k'}\frac{\partial \bar{u}_i}{\partial x_k}\right)}_{P_{ij}=\text{Stress Production}}\underbrace{-C_1\frac{\varepsilon}{k}\left[\overline{u_i'u_j'}-\frac{2}{3}\delta_{ij}k\right]-C_2\left[P_{ij}-\frac{2}{3}\delta_{ij}P\right]}_{\phi_{ij}=\text{Pressure Strain}}-\underbrace{\frac{2}{3}\delta_{ij}\varepsilon}_{\varepsilon_{ij}=\text{Dissipation}} \tag{3}$$

where the production term can be written as follows,

$$P_{ij}=-\left(\overline{u_i'u_k'}\frac{\partial \bar{u}_j}{\partial x_k}+\overline{u_j'u_k'}\frac{\partial \bar{u}_i}{\partial x_k}\right),\quad P=\frac{1}{2}P_{ii},\quad \delta_{ij}=\begin{cases}1(i=j)\\0(i\neq j)\end{cases} \tag{4}$$

where $\sigma_k=1.0$, $C_1=1.8$ and $C_2=0.6$ [27]. Moreover, the turbulence dissipation rate transport equation is given by,

$$\frac{\partial \varepsilon}{\partial t}+\bar{u}_j\frac{\partial \varepsilon}{\partial x_j}=\frac{\partial}{\partial x_j}\left[\left(\nu+\frac{\nu_t}{\sigma_\varepsilon}\right)\frac{\partial \varepsilon}{\partial x_j}\right]-C_{\varepsilon 1}\frac{\varepsilon}{k}\overline{u_i'u_j'}\frac{\partial \bar{u}_i}{\partial x_j}-C_{\varepsilon 2}\frac{\varepsilon^2}{k} \tag{5}$$

where $C_{\varepsilon 1}=1.44$, $C_{\varepsilon 1}=1.44$ and $C_{\varepsilon 2}=1.92$.

It was found that the turbulent air flow fields near the wall are crucial for accurately simulating particle deposition rates and behaviors [11]. The two-layer zonal model with enhanced wall function can improve the near-wall turbulent flow simulation accuracy [27]. The model can also be adopted here. More details of the model can be found in ANSYS FLUENT 13.0 [28].

For the inlet velocity boundary condition, the one seventh power law for velocity profiles was computed by [11],

$$U=U_{free}\left(\frac{y}{D/2}\right)^{1/7}\quad \text{for}\quad y\le D/2 \tag{6}$$

$$U=U_{free}\left(\frac{h-y}{D/2}\right)^{1/7}\quad \text{for}\quad y>D/2 \tag{7}$$

$$U_{free}=\frac{8}{7}U_{mean} \tag{8}$$

where D is the duct height and U_{mean} is the mean air velocity. The fully developed T.K.E. profiles were calculated by the following equations [11]. The dissipation rate of the T.K.E. was set as 1 m^2/s^3. The above inlet velocity and T.K.E. boundary conditions were imposed into duct inlet by UDF codes to ensure the fully developed turbulent status.

$$k=\frac{\tau_w}{\rho_g\sqrt{C_\mu}}+\frac{y}{D/2}\left(0.002U_{free}^2-\frac{\tau_w}{\rho_g\sqrt{C_\mu}}\right)\quad \text{for}\quad 0\le y\le D/2 \tag{9}$$

$$k=\frac{\tau_w}{\rho_g\sqrt{C_\mu}}+\frac{D-y}{D/2}\left(0.002U_{free}^2-\frac{\tau_w}{\rho_g\sqrt{C_\mu}}\right)\quad \text{for}\quad D/2<y\le D \tag{10}$$

$$\tau_w=\frac{\rho_g U_{mean}^2}{2}\cdot f \tag{11}$$

where f is the fanning friction factor,

$$f=0.0791\cdot \mathrm{Re}^{-0.25}\left(2{,}800<\mathrm{Re}<10^5\right) \tag{12}$$

where Reynolds number Re is defined as,

$$\mathrm{Re}=\frac{U_{free}h}{\nu} \tag{13}$$

Particle transport was simulated by discrete particle model (DPM). In this study, it is assumed that the particle air flows are dilute enough. Therefore, the influence of particle motions on turbulent

flow fields as well as particle–particle collisions are not considered here. Thus, the governing equation of particle movements is described as,

$$\frac{du_p}{dt}=\frac{1}{\tau}\frac{C_D\,\mathrm{Re}_p}{24}(u_g-u_p)+\frac{g(\rho_p-\rho_g)}{\rho_p}+\zeta\sqrt{\frac{\pi S_0}{\Delta t}}+\frac{2\rho K_c v^{0.5}}{\rho_p d_p(S_{lk}S_{kl})}s_{ij}(u-u_p) \tag{14}$$

where u_g is air velocity, u_p is particle velocity, ρ_g is air density, and ρ_p is particle density. The right hand of the equation is the drag force term, the gravity force and the buoyancy force term, the Brownian force term, and finally Saffman's lift force term. The particle relaxation time τ is calculated by,

$$\tau=\frac{Sd_p^2C_C}{18v} \tag{15}$$

S is the density ratio of particle to fluid. C_C is the Cunningham slip correction factor, computed as [29],

$$C_C=1+\frac{2\lambda}{d_p}\left(1.257+0.4e^{-(1.1d_p/2\lambda)}\right) \tag{16}$$

The drag coefficient C_D is calculated by,

$$C_D=\frac{24}{\mathrm{Re}_p},\quad \text{for}\quad \mathrm{Re}_p<1 \tag{17}$$

and

$$C_D=\frac{24}{\mathrm{Re}_p}(1+0.15\mathrm{Re}_p^{0.687}),\quad \text{for}\quad 1<\mathrm{Re}_p<400 \tag{18}$$

In the simulation, the inlet and outlet boundary conditions for the particles are "Escape", and the boundary conditions on the walls and the ribs for the particles are "Trap" [30]. In the realistic deposition process, a particle may either rebound from or remain attached to the surface when it impacts a surface [31]. Moreover, the attached particle may be re-suspended again in the air flow fields [32]. This process is very complicated. Nevertheless, in this study, the particle rebound and re-suspension are not considered. It is assumed that all the particles will be attached to the surface and will never be re-suspended once they impact the walls and ribs.

2.2. Turbulent particle dispersion

Turbulent dispersion of particles, caused by instantaneous turbulent fluctuation, is an important mechanism of particle dispersion and deposition [11]. In this simulation, Discrete Random Walk (DRW) was adopted to deal with turbulent particle dispersion. DRW model allows successive encounter of particles with turbulent eddies by a Gaussian distributed random velocity fluctuation of fluids and a time scale of turbulent eddy [33].

The instantaneous turbulent velocity fluctuation is calculated as follows,

$$u'=\zeta u'_{rms},v'=\zeta v'_{rms},w'=\zeta w'_{rms} \tag{19}$$

where u'_{rms}, v'_{rms} and w'_{rms} are velocity fluctuation, and ζ is normal distributed random number.

Previous studies showed that turbulent velocity fluctuation in the wall-normal direction has crucial influences on particle deposition velocity [11,26]. In this study, turbulent velocity fluctuation was corrected by UDF codes for both smooth and ribbed ducts. For smooth duct flow, the turbulent velocity fluctuation was corrected according to the DNS data by Tian and Ahmadi and Kim et al. [11,34].

$$\frac{v'_{rms}}{u^*}=C\left(y^+\right)^2,\quad \text{for}\quad y^+<4 \tag{20}$$

where u^* is the friction velocity and C is 0.008. y^+ is the non-dimensional distance from the wall, which is defined by,

$$y^+=\frac{yu^*}{v} \tag{21}$$

For ribbed duct flow, the correction equation for near-wall turbulent velocity fluctuation is shown as Eq. (22). The equation had been successfully applied in multilayer deposition simulation in ribbed channel flow by Lecrivain et al. [20].

$$\frac{v'_{rms}}{u^*}=\frac{a_1y^{+2}}{1+b_1y^++c_1y^{+2.41}},\quad \text{for}\quad y^+<30 \tag{22}$$

where $a_1=0.0116$, $b_1=0.203$ and $c_1=0.0014$.

2.3. Particle deposition velocity

Particle deposition velocity is defined by,

$$V_d=\frac{J}{C_0} \tag{23}$$

where J is the deposited particle number per unit time and unit surface area. C_0 is the mean concentration of particles. In the simulation, the particle deposition velocity V_d can be estimated by,

$$V_d=\frac{N_d/t/A}{N_0/V} \tag{24}$$

The particle deposition velocity is commonly non-dimensionalized by friction velocity,

$$V_d^+=\frac{V_d}{u^*} \tag{25}$$

where frictional velocity u^* can be computed by,

$$u^*=\sqrt{\tau_w/\rho_g}=U_{mean}\sqrt{f/2} \tag{26}$$

3. Case description and solution methods

Fig. 1(a) shows the two-dimensional (2D) smooth-wall duct. The duct size is 0.4 m long and 0.02 m high, which is consistent with the cases by Tian and Ahmadi [11], and Zhang and Chen [26] for further comparison. For ribbed ducts, the ribbed ducts with aligned and staggered arrangements are shown in Fig. 2(b) and (c), respectively. The first half of the duct was smooth to ensure that the air flow reaches full development state, while the second half of the duct is arranged by eighteen ribs with equal spacing on the walls. The rib pitch-to-height ratio p/e was also chosen as 10 and the rib height-to-duct diameter ratio e/D is 0.1. This is also in accordance with the experimental condition by Casarsa [35] for validating the flow fields in ribbed duct. Particle sizes in the simulation are 1, 2, 3, 5, 10, 20, 30 and 50 μm for both smooth and ribbed duct cases. Table 1 shows the detailed calculation cases. In present study, the air dynamic viscosity μ is 1.789×10^{-5} kg s/m. The air density is 1.225 kg/m^3 at $T=288$ K. The inlet air velocity is set as 5.5 m/s, thus the Reynolds number based on the mean air velocity and duct height is 7534. The density ratio of particle to fluid S is 2000. This is consistent with the literatures [11,26]. For each computational case, 30,000 spherical particles were released into the flow fields at X = 0.2

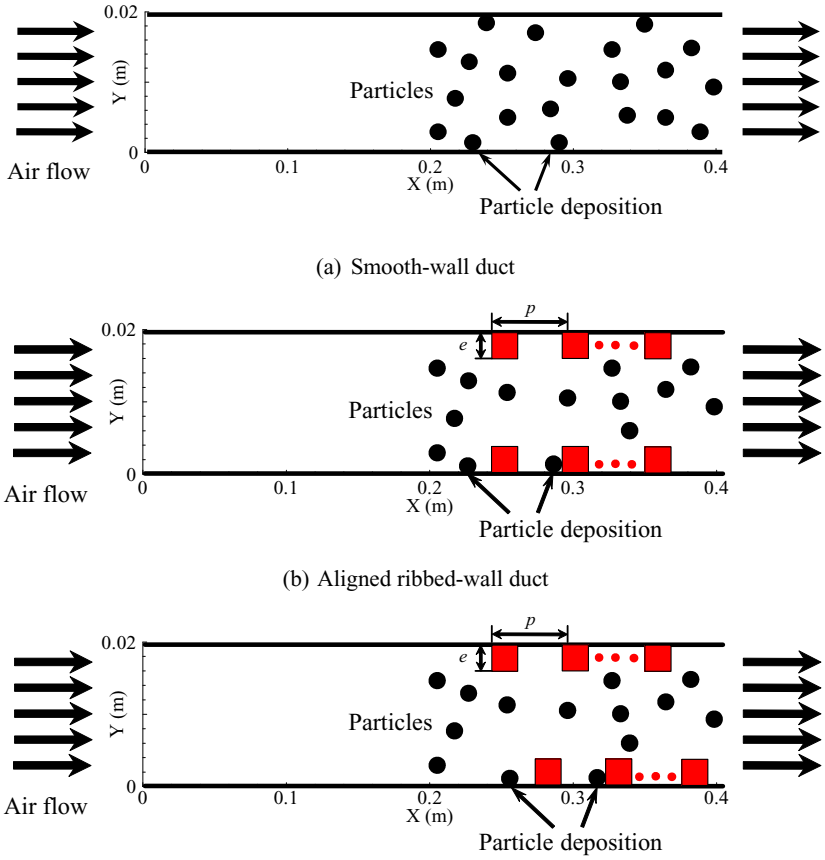

Fig. 1. Schematic of particle air flow in smooth, aligned ribbed and staggered ribbed ducts.

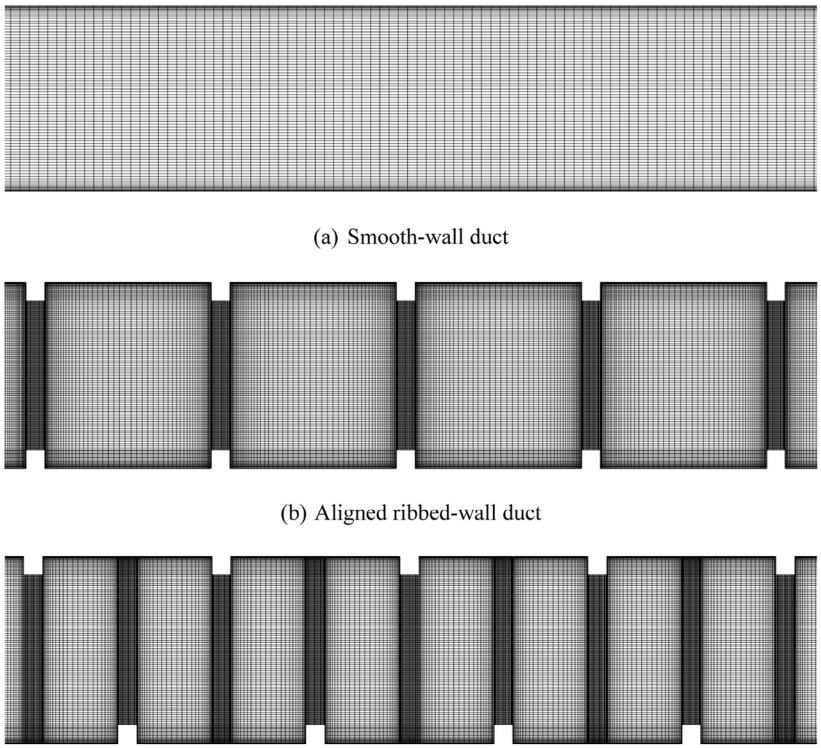

Fig. 2. Structural grids for smooth, aligned ribbed and staggered ribbed ducts.

Table 1
Computational cases.

Case no.	Air velocity (m/s)	Particle diameter (μm)	Surface type	Rib arrangement
A (1–8)	5.5 m/s	1, 2, 3, 5, 10, 20, 30, 50	Smooth	–
B (9–16)	5.5 m/s	1, 2, 3, 5, 10, 20, 30, 50	Ribbed	Aligned
C (17–24)	5.5 m/s	1, 2, 3, 5, 10, 20, 30, 50	Ribbed	Staggered

where the air flow was in fully developed state. The particle velocity was initially set as the mean air velocity. The gravity force was parallel with the air flow direction.

The computational domain for both smooth and ribbed duct cases was discretized by structured grids using ANSYS ICEM 13.0. To clearly display the structural mesh, the partial enlarged grids for a section of ducts are displayed in Fig. 2 for smooth, aligned ribbed and staggered ribbed duct cases. The grids are dense in near-wall and near-rib regions to accurately solve the complex air flow in turbulent boundary layers, as shown in Fig. 2. The first grid spacing from the walls and ribs is 0.05 m, which is about 1.13 dimensionless distance y^+. Then the grid spacing was enlarged to the center region with a growth factor 1.2. The total grid number is 32,000, 101,251 and 130,903 for smooth, aligned ribbed and staggered ribbed duct cases, respectively. The airflow governing equation was solved by the finite volume method (FVM). The convection term and the diffusion term were discretized by second-order upwind scheme and the second-order central difference scheme, respectively. The SIMPLE algorithm [36] was employed to decouple the velocity and pressure fields. Particle governing equations were solved by using the Runge–Kutta method. The turbulent velocity fluctuations correction, the inlet velocity and inlet T.K.E. profiles were all imposed into FLUENT by UDF codes.

4. Results and discussion

4.1. Numerical validation and air duct flow fields

The mean air flow velocity and fluctuating velocity profiles obtained at X = 0.3 m for smooth duct case were validated with direct numerical simulation (DNS) data by Kim et al. [34], as shown in Fig. 3(a) and (b). From Fig. 3(a), it can be observed that the mean air velocity profile obtained by the present RSM model with correction is in very good agreement with the DNS results. From Fig. 3(b), the velocity fluctuation profiles in streamwise and wall-normal directions also agree well with the DNS data. For aligned ribbed duct case, the air velocity profiles in ten streamwise positions from the 8th and 9th surface ribs were obtained and compared with experimental data by Casarsa [35], as shown in Fig. 4. It can be found that the air velocity profiles are consistent with the measurement results. The above agreements from Figs. 3 and 4 indicate that the present CFD models can resolve turbulent air flow very well for both smooth and ribbed duct cases.

Besides, the instantaneous air velocity fields for smooth and ribbed duct cases were shown in Fig. 5. From Fig. 5(a), the turbulent boundary layer for smooth duct flow can be observed very clearly. For ribbed duct cases, it can be seen that the periodic recirculation zones are produced by the surface ribs, and the turbulent boundary layers are raised away from the walls. Compared with the smooth duct case, the turbulent flow structures in the near-wall regions are significantly modified by the surface ribs. However, the difference between the aligned and staggered ribbed duct cases seems not obvious. Fig. 5 indicates that the air velocity fields and near-wall flow structures for smooth and ribbed duct cases were also simulated correctly by the present numerical methods.

Moreover, the dimensionless particle deposition velocity in smooth duct cases was obtained and compared with the literature data [11,26,37–44], as shown in Fig. 6. From the figure, it can be seen that the particle deposition velocity firstly increases rapidly with the increase of dimensionless particle relaxation time for several orders of magnitude. Then, it keeps almost constant with the particle relaxation time. This can be divided into two regimes: eddy diffusion-impaction regime and inertia-moderated regime. In the former regime, the particle deposition is determined by turbulent eddy diffusion combined with particle inertia. The deposition velocity in this regime would increase significantly with the particle relaxation time. In the latter regime, the particle deposition is mainly controlled by particle inertia. The deposition velocity would be

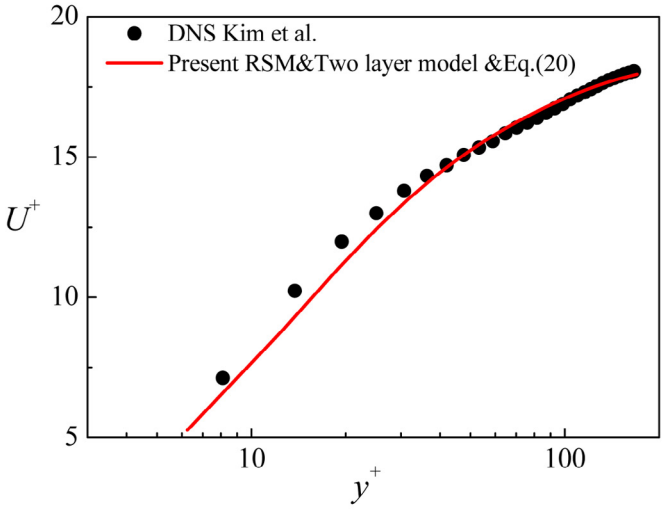

(a) Mean air flow velocity

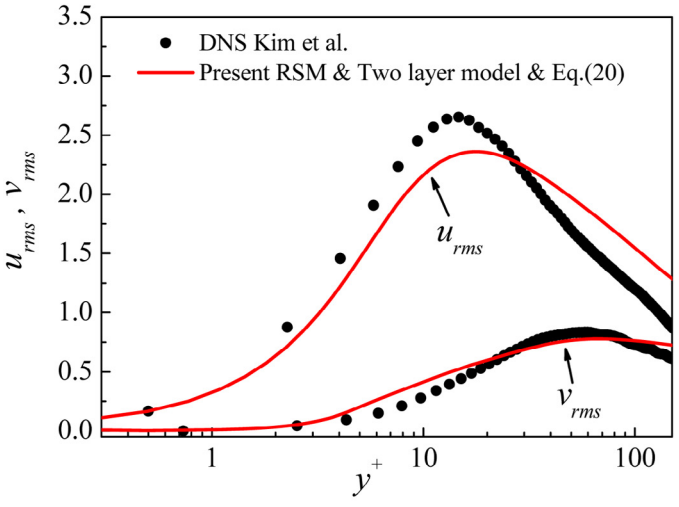

(b) Turbulent fluctuating velocity

Fig. 3. Validation of mean and fluctuating air velocity profiles with DNS data for smooth duct case.

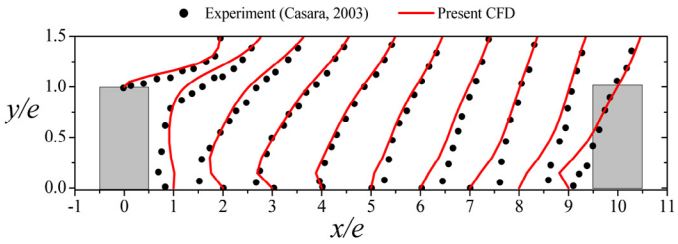

Fig. 4. Validation of air velocity profiles with experimental data for aligned ribbed duct case.

constant as the particle inertia has been large enough. It can be found that the deposition velocity profile obtained by the present simulation is in very good agreement with the literature data. This implies that the present methods can accurately predict particle deposition process in turbulent air flow.

4.2. Effects of different rib arrangements on particle deposition velocity

Fig. 7 compares the particle deposition velocities for smooth, aligned ribbed and staggered ribbed duct cases. It can be seen that particle deposition velocities are dramatically enhanced by surface ribs, compared with smooth duct case. Nevertheless, the enhancement ratios are significantly larger for small particles ($\tau_p^+ < 1$) than those for large particles ($\tau_p^+ > 1$). This is because the turbulent eddies produced by the surface ribs can easily capture small particle to deposition, but hardly entrain large particle with strong inertia. For the two rib arrangements, the particle deposition velocities seem to be very close in the logarithmic coordinates from Fig. 7. To quantitatively analyze the enhanced ratios of deposition velocity by surface ribs, an enhanced ratio γ was defined by,

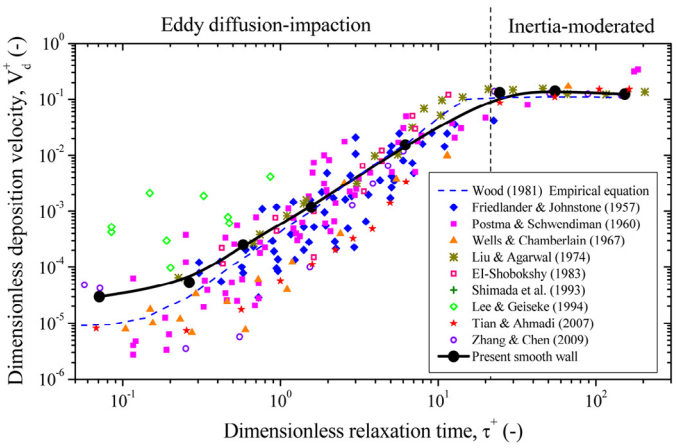

Fig. 6. Validation of particle deposition velocity with literature results for smooth duct case.

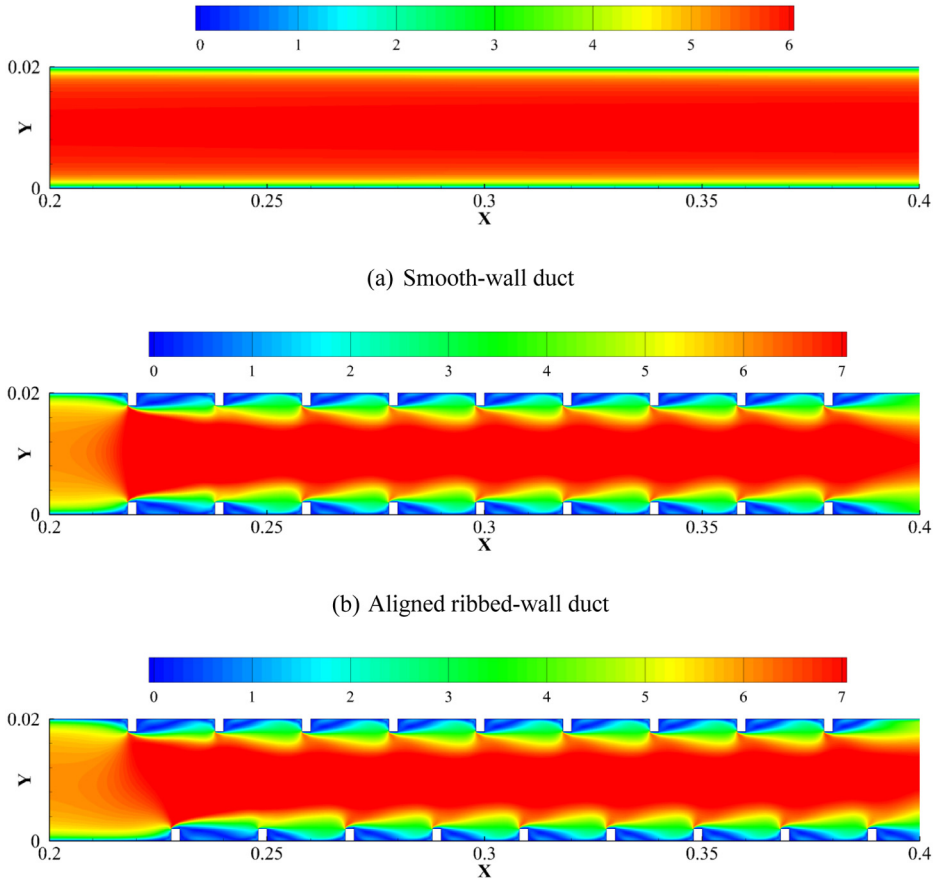

Fig. 5. Velocity fields and flow structures for smooth, aligned ribbed and staggered ribbed duct cases.

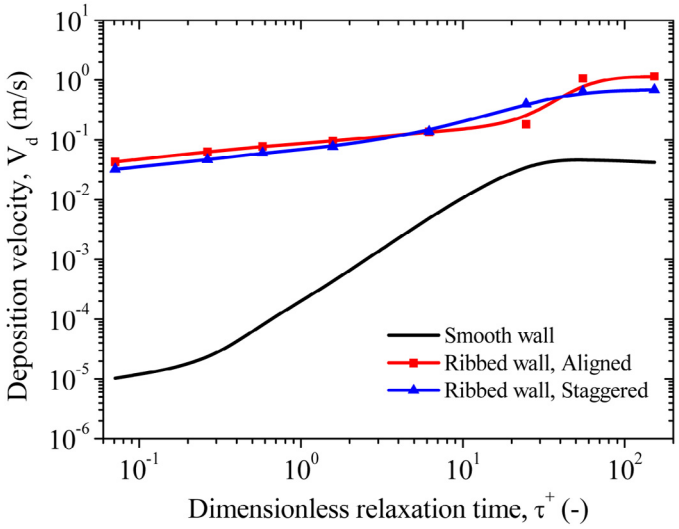

Fig. 7. Comparison of particle deposition velocities for smooth, aligned ribbed and staggered ribbed duct cases.

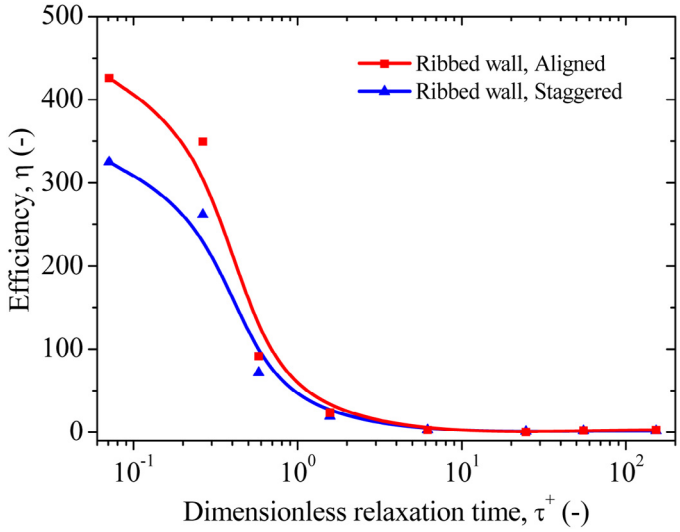

Fig. 9. Efficiency of particle deposition enhancement by aligned and staggered surface ribs.

$$\gamma = \frac{v_{drough}}{v_{dsmooth}} \tag{27}$$

Here, v_{drough} and $v_{dsmooth}$ represent the dimensional particle deposition velocity for ribbed and smooth duct cases, respectively. The enhanced ratios γ for aligned and staggered ribbed duct cases are shown in Fig. 8. A significant difference on the values of γ can be observed for small particle ($\tau_p^+ < 1$), while the enhanced ratios of deposition velocity are almost the same when particle relaxation time is larger than 1. For small particles ($\tau_p^+ < 1$), the surface ribs with aligned arrangement have better performance on particle deposition enhancement than the staggered one. The maximum enhanced ratio can reach 4200 for particle size 1 μm for aligned ribbed duct case, while it is 3150 for staggered ribbed duct case. For large particles ($\tau_p^+ > 1$), poor performance on deposition enhancement can be found for both rib arrangements. It implies that the aligned rib arrangement can enhance the particle deposition rate better than staggered arrangement, but the effects are just for small particles ($\tau_p^+ < 1$).

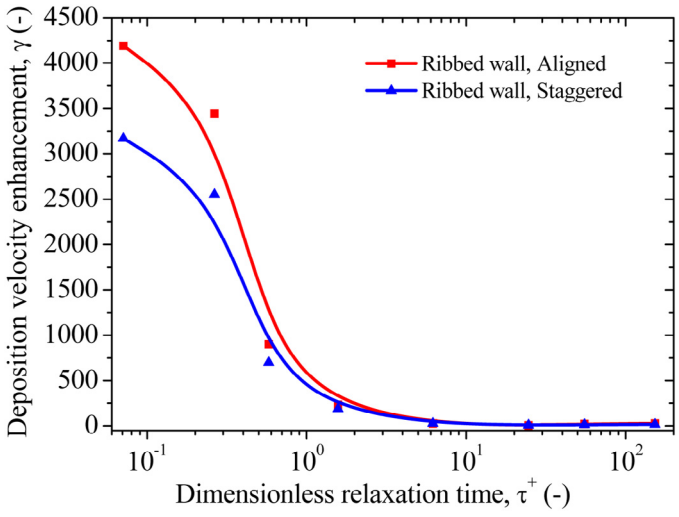

Fig. 8. Particle deposition enhancement ratios by surface ribs with aligned and staggered arrangements.

4.3. Particle deposition efficiency ratio for different rib arrangements

The advantage of surface ribs is the enhancement of particle deposition, but the flow drag is also increased by the ribs. It is necessary and important to consider both effects to evaluate the particle deposition efficiency ratio of the ribbed surface. The flow drag of the second half duct is respectively 0.0732, 0.7207 and 0.7139 *N* for smooth, aligned ribbed and staggered ribbed cases. Thus, the increase ratio of flow drag is 9.845 and 9.753 for aligned ribbed and staggered ribbed ducts, respectively. This indicates that the air flow drag is almost not influenced by the two different rib arrangements. The comprehensive efficiency for particle deposition enhancement was defined as follows,

$$\eta = \frac{v_{drough}}{v_{dsmooth}} \cdot \frac{f_{smooth}}{f_{rough}} \tag{28}$$

where f_{smooth} and f_{rough} are the air flow drag for smooth duct and ribbed duct, respectively.

The efficiency values for aligned and staggered ribbed ducts are shown in Fig. 9. Regarding the flow drag increase, the maximum enhancement efficiency ratio can reach 425 for particles with 1 μm diameter while the minimum enhancement efficiency ratio is just 2 for 20 μm particles for aligned ribbed duct cases. For staggered ribbed duct cases, the maximum efficiency is 325 also for 1 μm particles and the minimum efficiency is about 2 for 20 μm particles. The results show that surface ribs with aligned arrangement can enhance small particle deposition better with the same flow drag increase, while the surface ribs are not useful for large particle deposition enhancement.

5. Deposition enhancement mechanisms for different rib arrangements

To investigate the deposition enhancement mechanisms by surface ribs, Figs. 10 and 11 show the spatial distributions of active particles in smooth and ribbed ducts at $t = 0.03$ s for 1 μm and 50 μm particles, respectively. It is noted that the deposited particles are not displayed in the figures. The color of the particles represents particle velocity. The numbers and positions of deposited and active particles would be different for different time periods. Nevertheless, the comparison of the deposited and active particle numbers

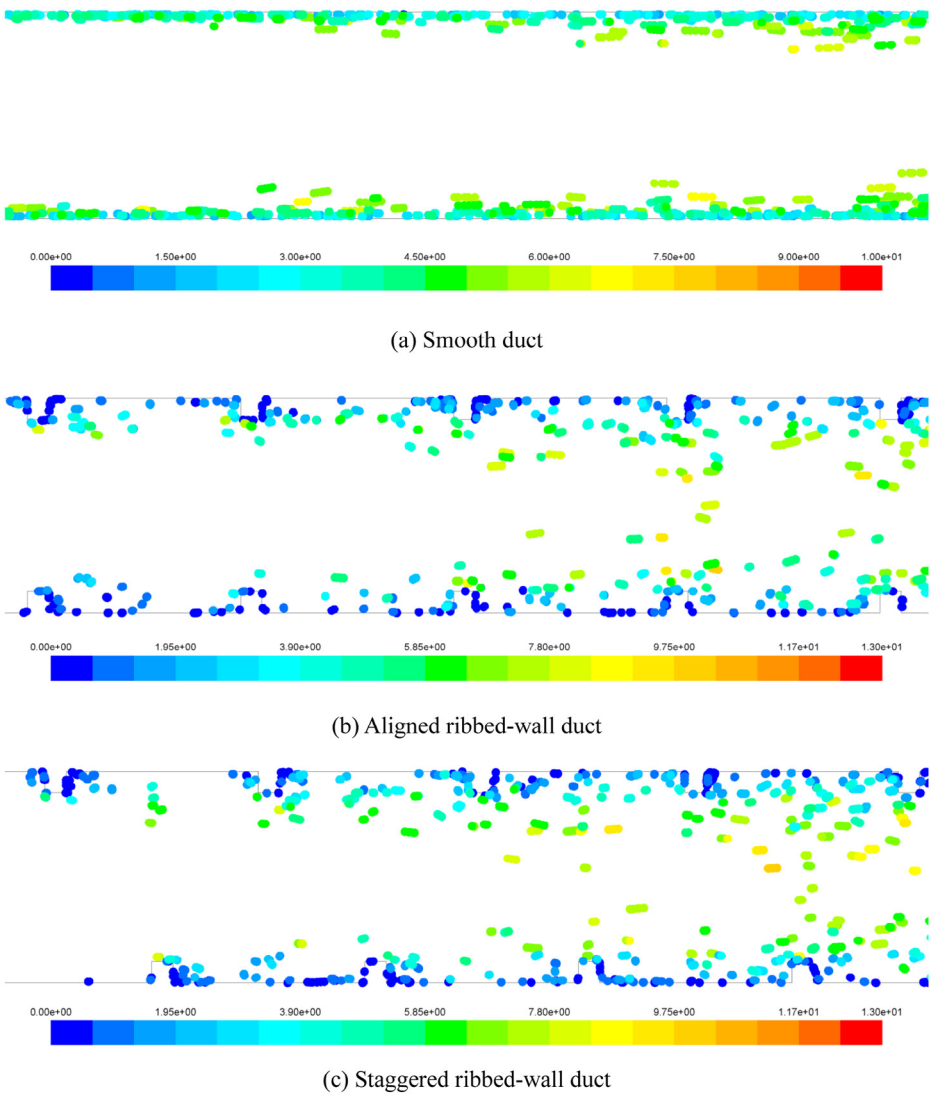

Fig. 10. Spatial distributions of active particles in smooth, aligned ribbed and staggered ribbed ducts for $d_p = 1$ μm.

in the same time period can indicate the deposition efficiency difference among the smooth, aligned ribbed and staggered ribbed duct cases. The particle number in Fig. 11 is obviously more than that in Fig. 10, because the deposition velocity for large particles is much larger than that for small particles. It can be found that a large number of particles are interpreted by the surface ribs, as shown in Figs. 10(b)-(c) and 11(b)-(c). Moreover, the surface ribs significantly increase the particle deposition area. Many particles are deposited on the projecting and side surfaces of the ribs. For smooth duct, the deposition area is 0.4 m in two dimensions. Meanwhile, it is 0.472 m for both aligned and staggered ribbed duct cases. The deposition area increase ratio can reach up to 18%. This can be beneficial for particle deposition enhancement. For large particles ($\tau_p^+ > 1$), the above two mechanisms are the main reasons to enhance particle deposition. As the two mechanisms are completely the same for aligned and staggered ribbed ducts, the deposition enhancement performance is very close for large particles by the two kinds of ribbed ducts.

However, for small particles ($\tau_p^+ < 1$), the capture and entrainment by turbulent eddies are important and have significant influence on particle deposition rate. Fig. 12 shows the T.K.E. distribution and streamlines of air flow in smooth, aligned ribbed and staggered ribbed ducts. It can be seen that a large separation eddy and a small reattachment eddy appear in the cavity between two adjacent surface ribs. The turbulent eddies induced by the ribs would capture the small particle and entrained them to the rib surface or the wall. At the same time, large T.K.E. is produced by the disturbance of surface ribs in the near-wall regions. Compared with smooth duct case, the T.K.E. values are dramatically enhanced in the regions above the surface ribs. This is favorable for particle turbulent dispersion and deposition. Therefore, the surface ribs have great performance on small particle deposition enhancement. For aligned ribbed and staggered ribbed duct cases, there are no obvious difference on the flow structures and T.K.E. values in the near-wall regions. The reason for different performance on small particle deposition enhancement may be the width of flow passage, as no other discrepancy can be found. The width of flow passage on the surface rib position is 0.018 m for aligned ribbed duct cases and 0.019 m for staggered ribbed duct cases. This may induce that more small particles are intercepted or captured by the turbulent eddies to deposit on the walls or rib surfaces. Therefore, the surface ribs with aligned arrangement can enhance small particle deposition better than that with staggered arrangement.

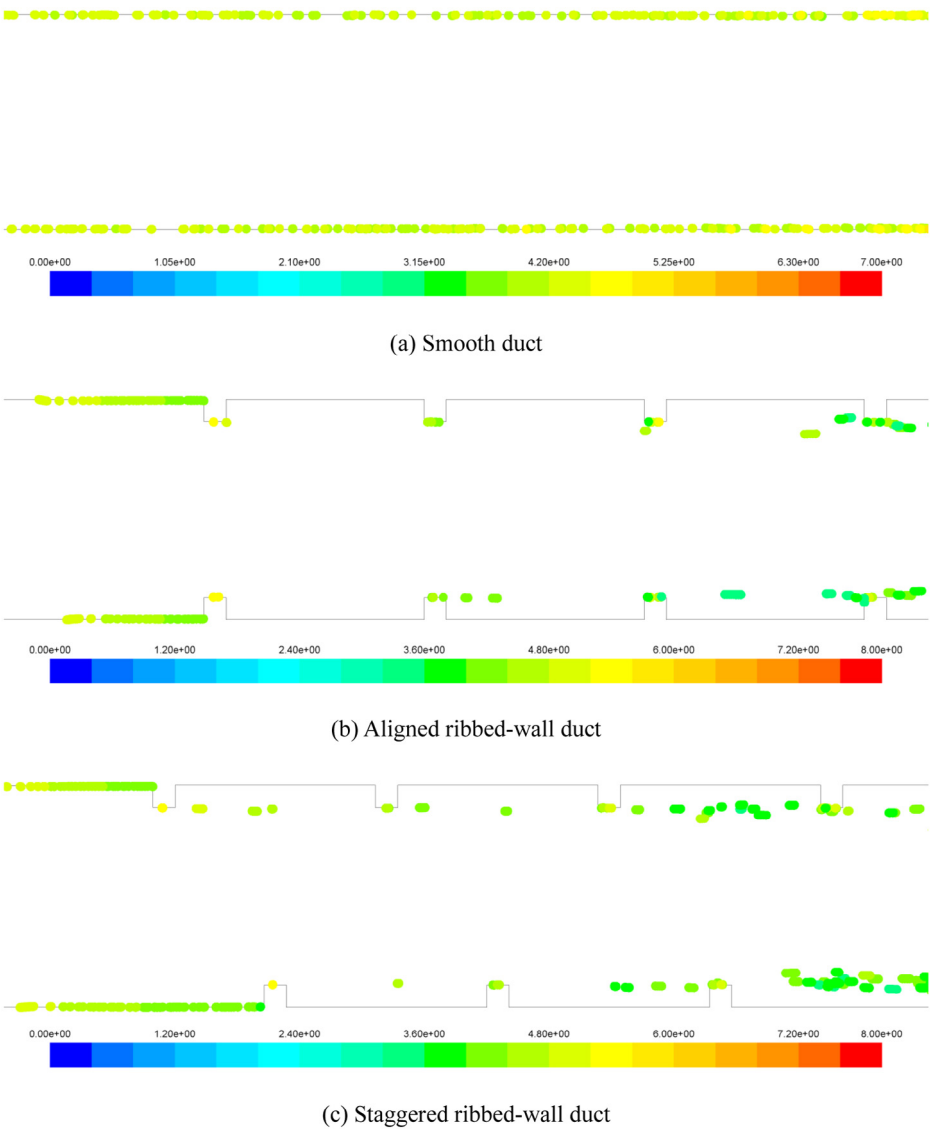

Fig. 11. Spatial distributions of active particles in smooth, aligned ribbed and staggered ribbed ducts for $d_p = 50$ μm.

6. Conclusions

Particle deposition in smooth, aligned ribbed and staggered ribbed duct air flows are studied and compared by RSM model with UDF correction and DPM model. The particle deposition enhancement considering the flow drag increase by the two surface ribs are investigated. Moreover, the mechanisms of particle deposition enhancement are analyzed and discussed. The following conclusions can be drawn.

1. The built numerical models (RSM model with UDF correction and DPM model) can accurately predict particle deposition rate and behavior in both smooth and ribbed turbulent duct air flows
2. The surface ribs with aligned arrangement can enhance particle deposition velocity better for small particles ($\tau_p^+ < 1$), compared with staggered ribbed duct case. For large particles ($\tau_p^+ > 1$),both surface ribs have poor performance on particle deposition enhancement. This is because large particles are difficult to capture and entrained by the near-wall turbulent eddies due to the large inertia.
3. The maximum pure particle deposition enhancement can reach 4200 for 1 μm particles for aligned surface ribs. Nevertheless, the flow drag is also increased for about 10 times by the surface ribs. Considering the flow drag increase, the comprehensive efficiency of particle deposition is 425 when particle size is 1 μm.
4. As the interception and deposition area increase, effects are completely the same for aligned and staggered ribbed duct, the mechanism that induces the different performance on small particle deposition enhancement may be the discrepancy on flow passage width on the surface rib position. Aligned ribbed duct has smaller flow passage width on the streamwise position of surface rib, therefore more small particles are captured by turbulent eddies and deposited on the rib surfaces or the walls.

In consequence, surface ribs with aligned arrangement are recommended to be applied in particle removal and air clean devices.

Acknowledgement

The authors appreciate the financial support provided by Central Policy Unit of the Hong Kong Government via the Public Policy Research Scheme (2013.A6.010.13A).

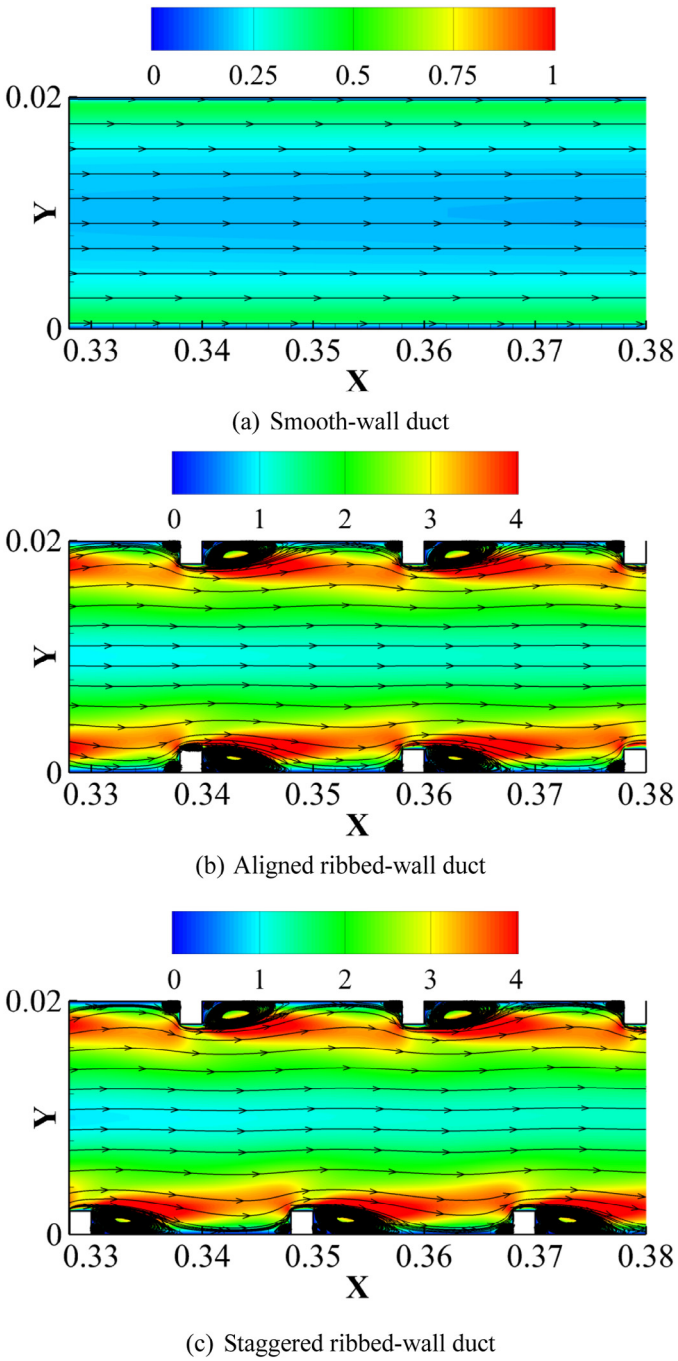

Fig. 12. T.K.E distribution and streamlines of air flow in smooth, aligned ribbed and staggered ribbed ducts.

References

[1] K.W. Cheong, Deposition of aerosol particles in ductwork, Appl. Energy 57 (1997) 253–261.
[2] T. Ma, M. Yan, M. Zeng, J.L. Yuan, Q.Y. Chen, B. Sunden, et al., Parameter study of transient carbon deposition effect on the performance of a planar solid oxide fuel cell, Appl. Energy 152 (2015) 217–228.
[3] F.D. Bellis, L.A. Catalano, CFD optimization of an immersed particle heat exchanger, Appl. Energy 97 (2012) 841–848.
[4] A. Li, G. Ahmadi, R.G. Bayer, M.A. Gaynes, Aerosol particle deposition in an obstructed turbulent duct flow, J. Aerosol Sci. 25 (1994) 91–112.
[5] M.A. Moon, M.J. Park, K.Y. Kim, Evaluation of heat transfer performances of various rib shapes, Int. J. Heat Mass Transf. 71 (2014) 275–284.
[6] H.Q. Zhang, H. Lu, B. Wang, X.L. Wang, Experimental investigation of flow drag and turbulence intensity of a channel flow with rough walls, Chin. Phys. Lett. 28 (8) (2011) 084703.
[7] J.H. Vincent, A.S.M. MacLennan, Aerodynamic considerations in electrostatic precipitator, J. Electrostatic 8 (1980) 325–342.
[8] H. Lu, L. Lu, Numerical investigation on particle deposition enhancement in duct air flow by ribbed wall, Build. Environ. 85 (2015) 61–72.
[9] H. Lu, L. Lu, Effects of rib spacing and height on particle deposition in ribbed duct air flows, Build. Environ. 92 (2015) 317–327.
[10] B. Zhao, J.J. Chen, Numerical analysis of particle deposition in ventilation duct, Build. Environ. 41 (2006) 710–718.
[11] L. Tian, G. Ahmadi, Particle deposition in turbulent duct flows – comparisons of different model predictions, J. Aerosol Sci. 38 (2007) 377–397.
[12] M.B. Othmane, M. Havet, E. Gehin, C. Solliec, Mechanisms of particle deposition in ventilation ducts for a food factory, Aerosol Sci. Technol. 44 (2010) 775–784.
[13] F. Chorel, A. Kondjoyan, P.S. Mirade, Toward quantitative CFD prediction of contaminant particle deposition against surfaces in large forced-ventilation food plants, Aerosol Sci. Technol. 44 (2010) 10–28.
[14] A.C.K. Lai, M.A. Byrne, A.J.H. Goddard, Measured deposition of aerosol particles on a two-dimensional ribbed surface in a turbulent duct flow, J. Aerosol Sci. 30 (1999) 1201–1214.
[15] A.C.K. Lai, M.A. Byrne, A.J.H. Goddard, Enhanced particle loss in ventilation duct with ribbed surface, Build. Environ. 35 (2000) 425–432.
[16] A.C.K. Lai, M.A. Byrne, A.J.H. Goddard, Aerosol deposition in turbulent channel flow in a regular array of three dimensional roughness elements, J. Aerosol Sci. 32 (2001) 121–137.
[17] G.I. Iacono, P. Tucker, A. Reynolds, Predictions for particle deposition from LES of ribbed channel flow, Int. J. Heat Fluid Flow 26 (2005) 558–568.
[18] Y.J. Suh, S.S. Kim, Effect of obstructions on the particle collection efficiency in a two-stage electrostatic precipitator, J. Aerosol Sci. 27 (1996) 61–74.
[19] T. Barth, M. Reiche, M. Banowski, M. Oppermann, U. Hampel, Experimental investigation of multilayer particle deposition and resuspension between periodic steps in turbulent flows, J. Aerosol Sci. 64 (2013) 111–124.
[20] G. Lecrivain, S. Drapeau-Martin, T. Barth, U. Hampel, Numerical simulation of multilayer deposition in an obstructed channel flow, Adv. Powder Technol. 25 (2014) 310–320.
[21] Q. Chen, Ventilation performance prediction for buildings: a method overview and recent applications, Build. Environ. 44 (4) (2009) 848–858.
[22] H. Jiang, L. Lu, K. Sun, Simulation of particle deposition in ventilation duct with a particle-wall impact model, Build. Environ. 45 (5) (2010) 1184–1191.
[23] K. Sun, L. Lu, H. Jiang, A computational investigation of particle distribution and deposition in a 90° bend incorporating a particle-wall model, Build. Environ. 46 (2011) 1251–1262.
[24] K. Sun, L. Lu, H. Jiang, A numerical study of bend-induced particle deposition in and behind duct bends, Build. Environ. 52 (2012) 77–87.
[25] N.P. Gao, J.L. Niu, Modeling particle dispersion and deposition in indoor environments, Atmos. Environ. 41 (2007) 3862–3876.
[26] Z. Zhang, Q. Chen, Prediction of particle deposition onto indoor surfaces by CFD with a modified Lagrangian method, Atmos. Environ. 43 (2009) 319–328.
[27] B.E. Launder, G.J. Reece, W. Rodi, Progress in the development of a Reynolds stress turbulent closure, J. Fluid Mech. 68 (3) (1975) 537–566.
[28] FLUENT Inc., FLUENT 12.0 User's Guide, Lebanon, NH, 2009.
[29] H. Ounis, G. Ahmadi, Analysis of dispersion of small spherical particles in a random velocity field, J. Fluids Eng. 112 (1990) 114–120.
[30] B. Zhao, Y. Zhang, X.T. Li, X.D. Yang, D.T. Huang, Comparison of indoor aerosol particle concentration and deposition in different ventilated rooms by numerical method, Build. Environ. 39 (2004) 1–8.
[31] B. Zhao, C. Chen, X.Y. Yang, A.C.K. Lai, Comparison of three approaches to model particle penetration coefficient through a single straight crack in a building envelope, Aerosol Sci. Technol. 44 (2010) 405–416.
[32] B. Zhou, B. Zhao, Z.C. Tan, How particle resuspension from inner surfaces of ventilation ducts affects indoor air quality – a modeling analysis, Aerosol Sci. Technol. 45 (2011) 996–1009.
[33] H. Jiang, L. Lu, K. Sun, Experimental study and numerical investigation of particle penetration and deposition in 90 degrees bent ventilation ducts, Build. Environ. 46 (2011) 2195–2202.
[34] J. Kim, P. Moin, R. Moser, Turbulence statistics in fully developed channel flow at low Reynolds number, J. Fluid Mech. 177 (1987) 133–166.
[35] L. Casarsa, Aerodynamic Performance Investigation of a Fixed Rib-roughened Internal Cooling Passage (Ph.D. thesis), Von Karman Institute for Fluid Dynamics, Belgium, 2003.
[36] S.V. Partankar, Numerical Heat Transfer and Fluid Flow, Hemisphere, Washington, DC, 1980.
[37] N.B. Wood, A simple method for the calculation of turbulent deposition to smooth and rough surfaces, J. Aerosol Sci. 12 (1981) 275–290.
[38] S.K. Friedlander, H.F. Johnstone, Deposition of suspended particles from turbulent gas streams, Ind. Eng. Chem. 49 (1957) 1151–1156.
[39] A.K. Postma, L.C. Schwendiman, Studies in micrometrics: I. Particle deposition in conduits as a source of error in aerosol sampling. Report HW-65308, Richland, Washington: Hanford Laboratory, 1960.
[40] A.C. Wells, A.C. Chamberlain, Transport of small particles to vertical surfaces, Br. J. Appl. Phys. 18 (1967) 1793–1799.
[41] B.Y.H. Liu, J.K. Agarwal, Experimental observation of aerosol deposition in turbulent flow, J. Aerosol Sci. 5 (1974) 145–155.
[42] M.S. El-Shobokshy, Experimental measurements of aerosol deposition to smooth and rough surfaces, Atmos. Environ. 17 (1983) 639–644.
[43] M. Shimada, K. Okuyama, M. Asai, Deposition of submicron aerosol particles in turbulent and transitional flow, AIChE J. 39 (1993) 17–26.
[44] K.W. Lee, J.A. Gieseke, Deposition of particles in turbulent pipe flows, J. Aerosol Sci. 25 (1994) 699–709.